

See discussions, stats, and author profiles for this publication at: <https://www.researchgate.net/publication/26801766>

# Doppler OCT imaging of cytoplasm shuttle flow in *Physarum polycephalum*

ARTICLE in JOURNAL OF BIOPHOTONICS · SEPTEMBER 2009

Impact Factor: 4.45 · DOI: 10.1002/jb.200910057 · Source: PubMed

CITATIONS

9

READS

41

## 4 AUTHORS:



Alexander V. Bykov

University of Oulu

64 PUBLICATIONS 224 CITATIONS

SEE PROFILE



Alexander Priezzhev

Lomonosov Moscow State University

191 PUBLICATIONS 927 CITATIONS

SEE PROFILE



Janne Lauri

University of Oulu

12 PUBLICATIONS 51 CITATIONS

SEE PROFILE



Risto A Myllylä

University of Oulu

418 PUBLICATIONS 4,129 CITATIONS

SEE PROFILE

FULL ARTICLE

# Doppler OCT imaging of cytoplasm shuttle flow in *Physarum polycephalum*

Alexander V. Bykov<sup>\*,1,2</sup>, Alexander V. Priezzhev<sup>\*\*,2</sup>, Janne Lauri<sup>1</sup>, and Risto Myllylä<sup>1</sup>

<sup>1</sup> University of Oulu, Optoelectronics and Measurement Techniques Laboratory, P.O. Box 4500, 90014 Oulu, Finland

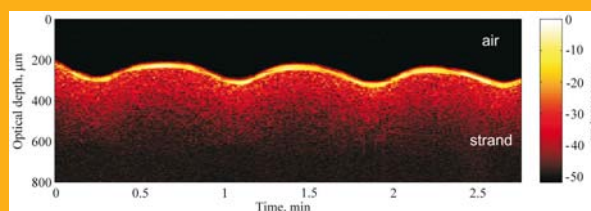
<sup>2</sup> M. V. Lomonosov Moscow State University, Physics Department and International Laser Center, 119991 Vorobiovy Gory, Moscow, Russia

Received 10 July 2009, revised 6 August 2009, accepted 6 August 2009

Published online 8 September 2009

**Key words:** Doppler OCT, *physarum*, cytoplasm, shuttle flow

The Doppler optical coherence tomography technique was applied to image the oscillatory dynamics of protoplasm in the strands of the plasmodium of slime mould *Physarum polycephalum*. Radial contractions of the gel-like walls of the strands and the velocity distributions in the sol-like endoplasm streaming along the plasmodial strands are imaged. The motility inhibitor effect of carbon dioxide on the cytoplasm shuttle flow and strand-wall contraction is shown. The optical attenuation coefficient of cytoplasm is estimated.



Time-resolved OCT pattern of *Physarum* strand-wall contractions. The thin yellow strip is the slime boundary between the air (above) and the strand (below). The lower boundary of the strand is not resolved due to strong scattering.

© 2009 by WILEY-VCH Verlag GmbH & Co. KGaA, Weinheim

## 1. Introduction

Optical coherence tomography (OCT) and its Doppler modification (DOCT) are nowadays rapidly developing tools for optical imaging. The progress in this field goes in several ways. The first way is the extension of the functionality and improving the technical characteristics such as resolution, sensitivity and imaging speed of the setup [1, 2]. Another way is the extension of the application field. The capability of imaging with high spatial and time resolution of the scattering media structure and flows

embedded into these media allows one to conduct detailed investigations of the structure and the functioning of the blood microcirculation system of humans or animals [3], imaging of embryonal development [4], as well as the study of cell motility dynamics [5, 6].

In this work, we report on the application of the DOCT technique for the imaging of cytoplasm shuttle flow in *Physarum polycephalum*. Slime mould *Physarum* [7] in the plasmodium phase of the life cycle is a unicellular organism representing a nonsta-

\* Corresponding author: e-mail: bykov@ee.oulu.fi, Phone: +358 8 553 2760, Fax: +358 8 553 2774

\*\* e-mail: avp2@mail.ru, Phone: +7 495 939 2612, Fax: +7 495 939 3113

tionary system of cylindrical strands which connect frontal zones of the migrating organism to the main body. Functionally, these strands resemble the blood capillary system. Inside the cell body the gel-like structures are continuously created and destroyed as a result of assemblage and dissociation of an actomyosin network. The local regions of such a network can spontaneously contract and relax causing the shuttle flows of the sol-like cytoplasm. One of the interesting features of biological motility of *Physarum* is its oscillating nature. *Physarum* shows the complex autowave amoeboid type of cellular motility including the cyclic contraction of the gel-like walls of the strands. These contractions generate the gradients of pressure, which cause shuttle flow of the internal part of the cytoplasm along the strands. The typical period of oscillation of a strand with a diameter of about several hundred micrometres at room temperature is about 1 min.

The dynamics of the wall contraction and the cytoplasm shuttle flow in *Physarum* have been studied by numerous researchers implementing phase-contrast microscopy [8], laser Doppler microscopy [9, 10] and image analysis [11] aiming, in particular, to assess the mechanism of synchronization of the oscillations and the nature of the pacemaker and synchrofactor. Mathematical models have been designed to describe complex dynamic phenomena [9, 12]. However, many problems have not been solved so far due to limited possibilities of the applied measurement techniques. Laser Doppler microscopy, in particular, to say nothing about standard microscopy, did not allow for simultaneous patterning of quasi-instantaneous in-depth profiles of the streaming velocities and strand contractions along with their temporal evolutions during successive contraction–relaxation cycles. We have not heard of any attempts to apply the novel micro-PIV (particle image velocimetry) technique that could possibly be applicable for this purpose. However, the size of computer memory that might be needed for collecting the necessary amount of data might be too high. In these circumstances, DOCT is an advantageous technique for more deeply assessing the interrelations of structural and dynamic alterations in the plasmodial cytoplasm, which form the basis for the variety of autowave phenomena in this object.

The present work is the first, to our knowledge, attempt to study *Physarum* with the DOCT technique with high spatial and velocity resolution.

It is important to note that many tissue cells of animals and humans (e.g. cancer cells) exhibit an amoeboid type of motility; thus, more detailed assessment of its motion is an important task for developing the theoretical basis of nonmuscle biological mobility and for medical applications in particular.

## 2. Materials and methods

### 2.1 Measuring setup

The laboratory-built DOCT system [13] is based on a free-space Michelson interferometer (see Figure 1). It utilizes a superluminescent diode (SLD) with a central wavelength of 840 nm and a spectral band of 50 nm (full width at half maximum) as the light source. Determined by these parameters, the depth resolution of the system is  $\Delta z = 6.2 \mu\text{m}$  in air and  $\Delta z/n_{\text{cyt}} = 4.5 \mu\text{m}$  in cytoplasm, where  $n_{\text{cyt}}$  is the refractive index of cytoplasm [14]. Placed on a piezo translation stage, the measurement setup is capable of performing very accurate and repeatable scans. Light from the SLD is first collimated and then transferred through an optical isolator to prevent optical feedback. The beam is divided by a 50/50 cube beam splitter (BS) to form a reference arm and a measurement arm. In both arms, the beam is focused by a focusing lens (FL) with a focal length of 65 mm and a diameter of 10 mm. Different from the conventional time-domain DOCT, the mirror of the reference arm is fixed relative to the other components in the measurement setup. Depth scanning is performed by moving the scanning stage with the whole measurement setup on top of it. This type of scanning was chosen to minimize the number of moving parts and to achieve better lateral resolution by moving the focus point during scanning. In addition to the better lateral resolution, tracking the focus point also improves the signal-to-noise ratio of the setup. The interference signal resulting from mixing the light scattered consecutively at different depths of the strand by the optical nonhomogeneities of cytoplasm (mostly nuclei and mitochondria) with the

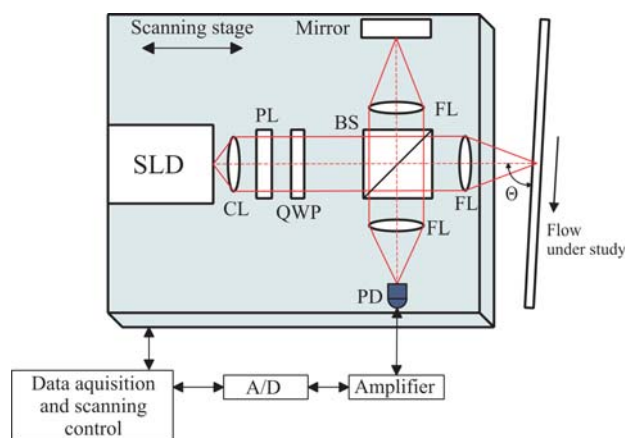


**Figure 1** (online color at: [www.biophotonics-journal.org](http://www.biophotonics-journal.org)) Schematic layout of the DOCT setup. SLD – superluminescent diode, CL – collimator, PL – polarizer, QWP – quarter-wave plate, BS – beam splitter, FL – focusing lens, PD – photodiode.



**Figure 2** (online color at: [www.biophotonics-journal.org](http://www.biophotonics-journal.org)) Photo-image of *Physarum* strands lying on an agar layer in a Petri dish.

reference beam is measured by a silicon PIN photodiode (PD). The output current is first converted to a voltage signal by a transimpedance preamplifier. Then, the analogue voltage signal is filtered and amplified with a voltage amplifier, before being transferred to a 12-bit AD converter at the 100 kHz sampling frequency. During the measurements the speed of the scanning stage was 1.6 mm/s, which corresponds to a carrier frequency of 3810 Hz. The present setup allows for measuring the flow velocities in the range from 0.1 to 3 mm/s. The upper limit of this range is determined by choosing the upper filter limit, which can be adjusted depending on our demands.

## 2.2 Object preparation

Plasmodium of *Physarum polycephalum* was grown on filter paper or agar gel and fed with oat flakes at room temperature of 23 °C in the dark according to [15]. Ten hours before the measurements, a piece of filter paper with *Physarum* biomass on it was placed into a Petri dish with the diameter of 5.5 cm close to the border. The piece of filter paper with wet oat flakes was placed on the diametrically opposite side of the dish to attract the *Physarum* and make its migration directed. The bottom of the Petri dish was covered with an agar layer about 1 mm thick. During about 10 h *Physarum* was allowed to move on the agar surface to form a strand network. Figure 2 shows as an example two strands connecting the larger parts of the *Physarum* spread upon two pieces of filter paper with oat flakes.

## 3. Results and discussion

### 3.1 OCT imaging

The Petri dish with the plasmodium was placed into the measuring arm of the setup perpendicular to the probing beam. All the measurements were carried out at room temperature of 23 °C. The in-depth

scanning was performed in a single point of the selected strand (upper strand in Figure 2). Several consecutive A-scans were placed one by one along the time axis to form a time-resolved pattern resulting from the alteration of the strand thickness during the contraction–relaxation cycle in the point of scanning. In Figure 3 one can see the obtained OCT patterns of the *Physarum* strand at different activity regimes within its life cycle. In Figure 3a and b one can see the OCT patterns of local contractions of a strand with the diameter of about 300 μm. It is possible to distinguish the time course of the strand's outer boundary in the point of scanning (yellow wavy band) from the inner part of the cytoplasm (region below the upper wall), to clearly see the contraction and to determine its amplitude and period. However, in these patterns, the rear border of the strand is seen not to be clearly distinguished because of a very small difference between the refractive indices of the cytoplasm and the agar–agar gel and strong light scattering by cytoplasm.

In the course of migration of the plasmodium the contractile activity of a certain strand may decrease and the strand itself may become thinner. This case is shown in Figure 3c and d. Here the contractions are very weak; however, one can see more clearly the rear wall. Thus, the OCT technique allows one to perform local monitoring of different contractile activity regimes of the *Physarum* life cycle and thus to get better insight into the mechanisms of its machinery.

### 3.2 Doppler OCT imaging

To perform the Doppler measurements the angle between the probing beam and the selected strand was set to 40 degrees. The velocity of the flow was calculated according to the formula

$$V = \frac{(f_D - f_C) \lambda}{2n_m \cos \theta},$$

where  $\lambda$  is the central wavelength of the SLD,  $f_D$  is the measured Doppler frequency,  $f_C$  is the carrier Doppler frequency from the scanning mirror or the movement of the stage,  $n_m$  is the mean refractive index of the medium, which in the case of cytoplasm was supposed to be 1.38 [14], and  $\theta$  is the Doppler angle.

Analogously to the OCT patterns described above, several consecutive flow velocity profiles were placed one by one along the time axis to represent the temporal variations of the cytoplasmic flow. A typical result of measurements is shown in Figure 4. From this figure one can see the so-called shuttle flow of cytoplasm inside the strand as well as



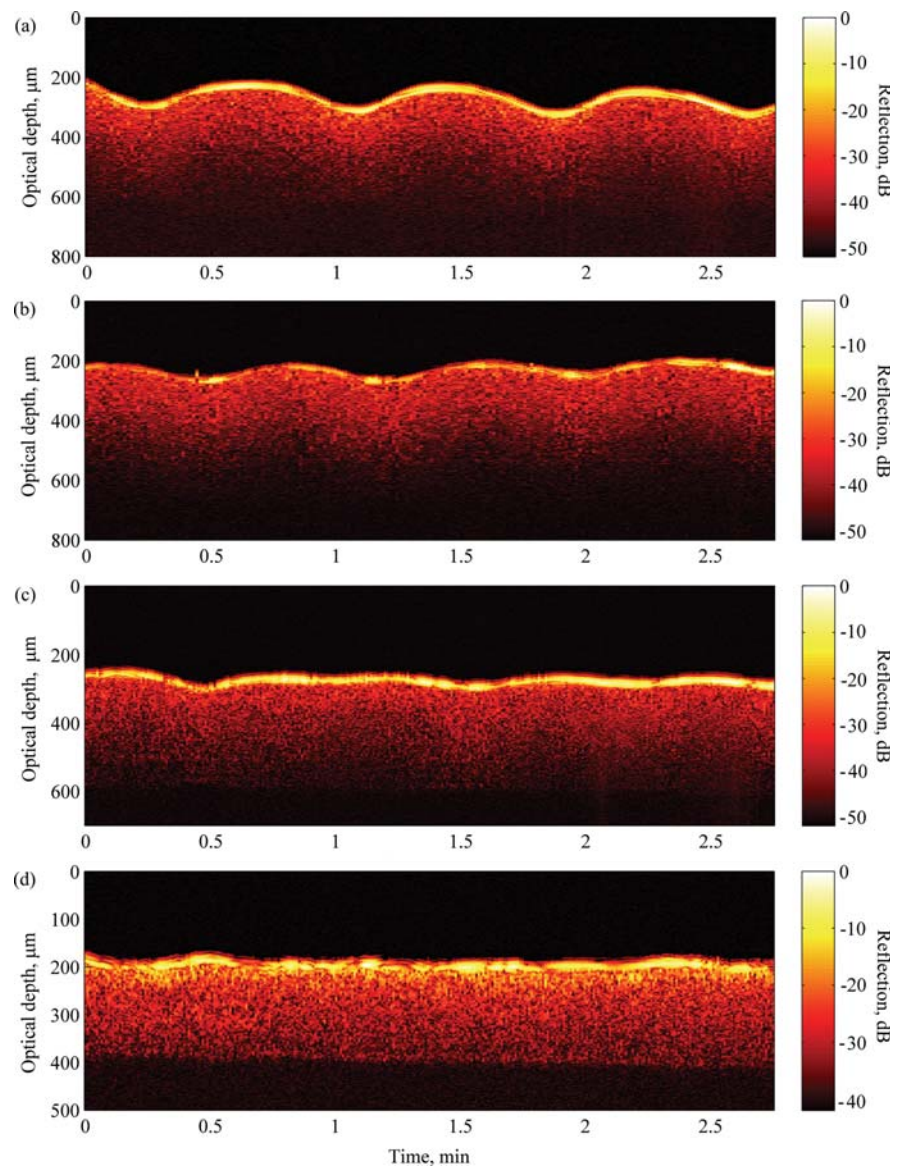


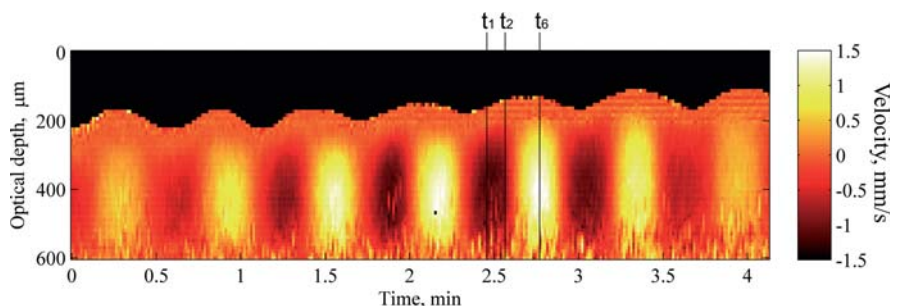
**Figure 3** (online color at: [www.biophotonics-journal.org](http://www.biophotonics-journal.org)) Time-resolved OCT patterns of the *Physarum* strand pulsations at different activity regimes.

the contraction of its upper wall. Dark spots and light spots are negative and positive flow directions, respectively. Zero velocity corresponds to a light-red colour.

From this picture, it is possible to obtain the dynamic characteristics of the flow at different depths inside the strand with high velocity resolution. For

example, in Figure 5 derived from Figure 4 one can see the time dependence of the axial velocity (velocity in the centre of the strand)  $V_{\max}(t)$ . The low-frequency modulation of the velocity oscillation is well seen. This modulation is a consequence of the distributed and self-oscillating nature of *Physarum* contraction activity [9].

**Figure 4** (online color at: [www.biophotonics-journal.org](http://www.biophotonics-journal.org)) Time-resolved DOCT pattern of *Physarum* strand dynamics. Besides the velocity variations one can also see the contractions of the upper border of the strand wall.



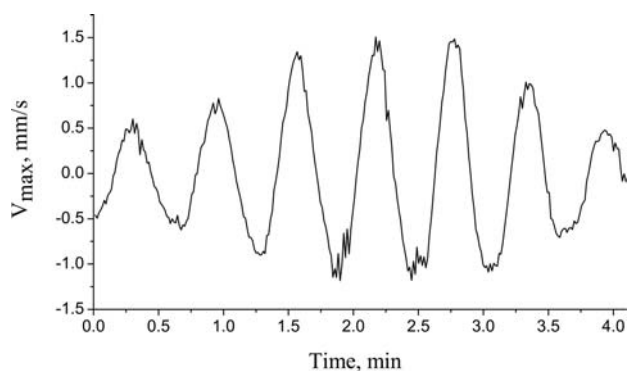


**Figure 5** Time dependence of local cytoplasmic streaming velocity variations in the centre of the strand.

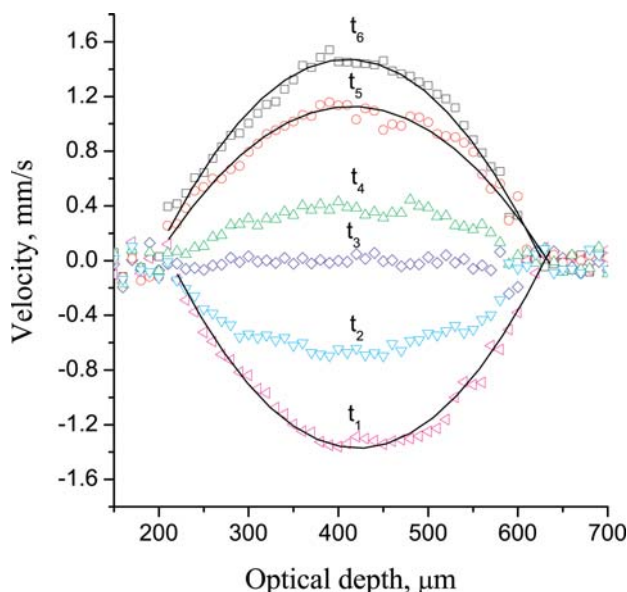


**Figure 6** (online color at: [www.biophotonics-journal.org](http://www.biophotonics-journal.org)) Cytoplasmic flow velocity profiles at different time instances  $t_1, \dots, t_6$ . Solid lines – parabolic approximations of the measurement data.

In Figure 6 several flow velocity profiles measured at different time instances corresponding to  $t_1, \dots, t_6$  in Figure 4 are depicted. From this picture one can clearly see that the parabolic approximations (solid lines) fit pretty well to the measured velocity profiles. In accordance with this fact, we can claim that non-Newtonian behaviour of cytoplasm in the strands of such diameters is negligible.

### 3.3 Effect of mobility inhibitor (carbon dioxide) on cytoplasmic streaming

We applied DOCT imaging to test the feasibility of studying the effect of carbon dioxide on the cytoplasmic streaming. Carbon dioxide is one of the inhi-

bitors of nonmuscle mobility which blocks the contraction and stops the cytoplasm flow. The gas was pumped through the Petri dish. The pumping rate was chosen with the assumption that the gas jet should have no mechanical influence on the *Physarum* strand. After the contractions were stopped the gas flow was also immediately stopped and  $\text{CO}_2$  started to slowly run out from the dish. The patterns showing this process are presented in the Figure 7 and 8. It is clearly seen how the carbon dioxide stops the flow. After the elimination of  $\text{CO}_2$ , the shuttle flow and the wall contractions slowly recover.

### 3.4 Scattering properties of cytoplasm

The OCT technique also gives us a unique possibility to determine the scattering properties of the object under study *in vivo*. According to the OCT signal formation theory [16], the slope of the OCT signal carries information about the scattering properties of the medium under study, such as scattering and absorption coefficients. Several research groups [17–19] have reported the possibility of determining the optical properties of scattering media by the OCT technique using rather complicated theories of OCT signal formation. This approach was used to monitor the glucose level in biotissues *in vivo* [20, 21]. In our study, we have also made an attempt to determine the scattering coefficient of the cytoplasm in the *Physarum plasmodium* strand from the obtained OCT scans. In Figure 9 one can see the linear parts of the normalized OCT signals from Figure 3 plotted in logarithmic scale. To suppress the OCT speckles, averaging over 200 samples of the obtained signals was performed. Since the surface of the object under study is oscillating it is necessary to align the obtained A-scans before averaging. Such kind of alignment was performed by shifting the A-scans to a certain common position of the origin of the OCT signals. Before the speckle-noise reduction, the standard deviation of the OCT signal increased from 10 to 60% for near-surface and deeper parts of the signal correspondingly. The averaging allows reducing these values to 3 and 15% correspondingly. The depth values were recalculated from the measured optical depth values by division by the cytoplasm refractive index. The scattering coefficient was calculated as the tangent of the slope angle of the linear fit of the obtained signals. This method of the scattering coefficient determination is valid in the assumption that only single-scattered photons are contributing to the OCT signal, which is true for the considered parts of the signals in our case. Another assumption is that the absorption coefficient should be negligible in comparison with the scattering coefficient. This criterion is usually fulfilled for most biotissues in the near-infrared range of wavelengths.

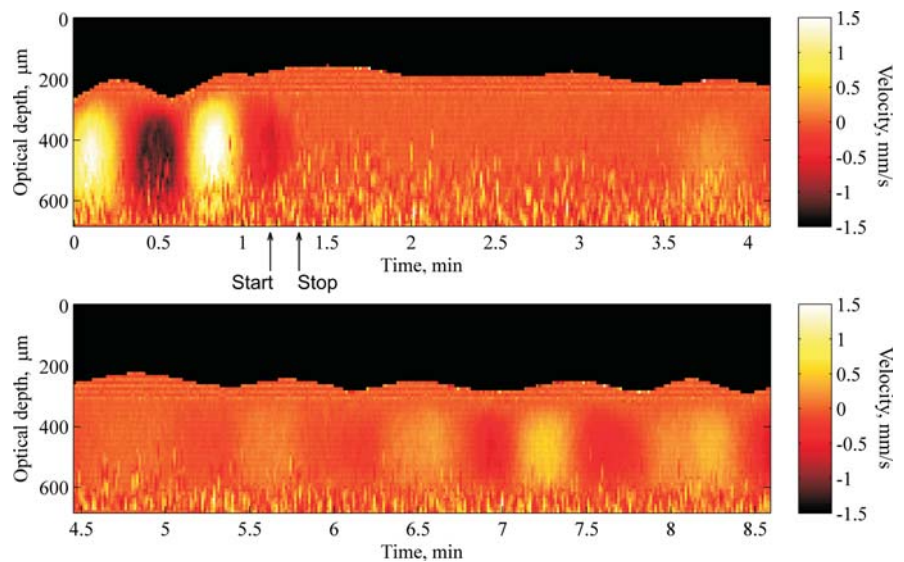


**Figure 7** (online color at: [www.biophotonics-journal.org](http://www.biophotonics-journal.org)) Time-resolved DOCT pattern of *Physarum* strand dynamics briefly subjected to the influence of CO<sub>2</sub>. The black arrows on the time axis show the moments of the beginning and the end of CO<sub>2</sub> pumping.

The 2% Intralipid solution with known scattering coefficient was used as the reference to validate the procedure of parameter determination. Intralipid [22, 23] is a polydisperse suspension of almost spherical particles of about 0.3 μm mean radius suspended in glycerine and water solution. The particles are soyabean oil droplets covered with a 2.5–5.0 nm-thick lipid membrane. In the field of biomedical optics, this liquid is frequently used for the fabrication of tissue phantoms. The results of the estimation of the scattering coefficient are shown in Figure 9. For the 2% Intralipid solution the measured coefficient  $\mu_s$  is  $5.4 \pm 0.4 \text{ mm}^{-1}$ . According to the van Staveren approximation [23], the scattering coefficient of the 2% Intralipid solution at the wavelength of 840 nm is  $\sim 5 \text{ mm}^{-1}$ , which corresponds well to the value obtained in our measurements. Thus, we can be sure that our method gives correct results. For the *Physarum* strands the values of the scattering coefficient measured at different activity

regimes range from  $12 \pm 1$  to  $19 \pm 2 \text{ mm}^{-1}$ . The difference in the mean values of  $\mu_s$  corresponding to different activity regimes noticeably exceeding the standard deviations may be due to structural changes in the strand leading to changes in its local optical properties.

## 4. Conclusions

We showed that modern OCT and DOCT techniques have a potential of yielding more informative experimental data on *Physarum* dynamics than conventional techniques used in earlier studies. OCT allows for obtaining cross sections of the plasmodium strands with spatial resolution of about several mi-

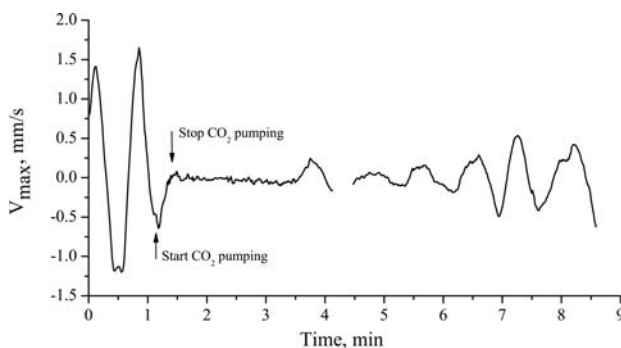


**Figure 8** Time dependence of the axial velocity of cytoplasm flow in the *Physarum* strand before, during and after the influence of CO<sub>2</sub>. The moments of the beginning and the end of gas pumping are shown with the black arrows.

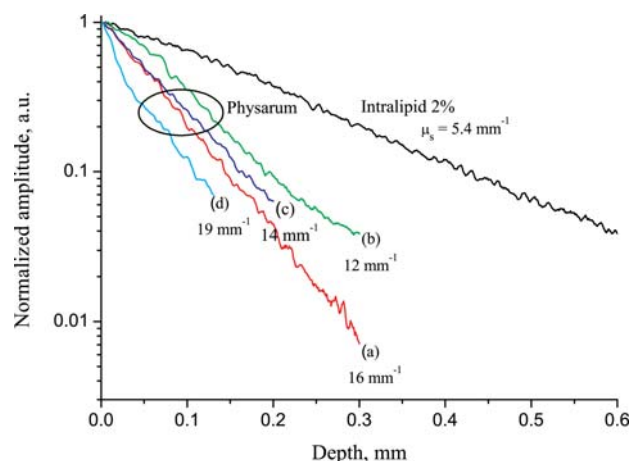


**Figure 9** (online color at: [www.biophotonics-journal.org](http://www.biophotonics-journal.org)) The averaged OCT signals used for the estimation of the scattering coefficient. (a)–(d) correspond to the cases shown in Figure 3.



chrometres and conducting *in vivo* measurements of their thickness simultaneously with local imaging of the strand-wall contractions. From the obtained patterns it is also possible to determine the scattering coefficient of the strands, which in our case is in the range from 12 to 19 mm<sup>-1</sup>. DOCT allows for investigating the protoplasm shuttle streaming in more detail, in particular determining the flow velocity profiles with high spatial resolution at the same time with imaging of wall contractions. We believe that these possibilities will give an impetus to further studies of the complex nonmuscle mobility of *Physarum* and other live objects with amoeboid type of locomotion.

**Acknowledgements** This work was supported by grants of the Academy of Finland, the Russian Foundation for Basic Research (No. 08-02-91760-AΦ a) and Infotech Oulu (Finland). Alexander Bykov acknowledges GETA Graduate School. The authors thank Prof. Yu. M. Romanovsky for useful discussions and Dr. S. I. Beilina for providing us with sclerotia of *Physarum* and consultations on *Physarum plasmodium* cultivation.



**Alexander V. Bykov** is a Dr. Tech. student in the Optoelectronics and Measurement Techniques Laboratory of the University of Oulu, Finland. He graduated with honours in 2005 from the Physics Department of Moscow State University and received his Ph.D. degree in 2008 from the same university.

His scientific interests are in the areas of biophotonics, noninvasive optical diagnostics, theory of light propagation in scattering media including biotissues and numerical simulation of light transport.



**Alexander V. Priezzhev** graduated from the Physics Department of Lomonosov Moscow State University (MSU) in 1971 and earned his Ph.D. degree in physics and mathematics from MSU in 1975. His current position is professor and head of the Biomedical Photonics Laboratory at the Physics Department of MSU. He is also adjunct professor of the

School of Biomedical Engineering, Science and Health Systems at Drexel University, USA. He is co-author of

more than 250 peer-review articles, invited talks and conference proceedings papers and several books and book chapters related to laser physics, biomedical optics and laser applications in biology and medicine.



**Janne Lauri** graduated with a Master's degree from the University of Oulu, Finland in 2007. He did his Diploma thesis on flow velocity profile measurements with Doppler OCT. Now he is a Ph.D. student in the Optoelectronics and Measurement Techniques Laboratory, University of Oulu. He is currently working with flow velocity measurements with industrial suspensions as well as biomedical suspensions to characterize fluid flow properties. His research interests also include structure measurements with optical coherence tomography.



**Risto Myllylä** received the D.Sc. (Eng) degree from the University of Oulu, Finland, in 1976. He has been an associate professor in the Department of Electrical Engineering, University of Oulu, since 1974 and a professor since 1995. From 1988 to 1995 he was a research professor in the Technical Research Centre of Finland. His research interests include industrial and biomedical instrumentation development, particularly in optical measurements. He has co-authored two books and more than 500 papers and patents. Dr. Myllylä is a past president of the Finnish Optical Society and an Advisory Committee Member of the European Optical Society (EOS).

His research interests include industrial and biomedical instrumentation development, particularly in optical measurements. He has co-authored two books and more than 500 papers and patents. Dr. Myllylä is a past president of the Finnish Optical Society and an Advisory Committee Member of the European Optical Society (EOS).

## References

- [1] E. J. Fernández, B. Hermann, B. Považay, A. Unterhuber, H. Sattmann, B. Hofer, P. K. Ahnelt, and W. Drexler, Ultrahigh resolution optical coherence tomography and pancorrection for cellular imaging of the living human retina, *Opt. Express* **16**, 11083–11094 (2008).
- [2] M. Y. Jeon, J. Zhang, Q. Wang, and Zh. Chen, High-speed and wide bandwidth Fourier domain mode-locked wavelength swept laser with multiple SOAs, *Opt. Express* **16**, 2547–2554 (2008).



- [3] B. White, M. Pierce, N. Nassif, B. Cense, B. Park, G. Tearney, B. Bouma, T. Chen, and J. de Boer, In vivo dynamic human retinal blood flow imaging using ultra-high-speed spectral domain optical coherence tomography, *Opt. Express* **11**, 3490–3497 (2003).
- [4] M. W. Jenkins, O. Q. Chughtai, A. N. Basavanahally, M. Watanabe, and A. M. Rollins, In vivo gated 4D imaging of the embryonic heart using optical coherence tomography, *J. Biomed. Opt.* **12**(3), 030505, 1–3 (2007).
- [5] M. A. Choma, A. K. Ellerbee, S. Yazdanfar, and J. A. Izatt, Doppler flow imaging of cytoplasmic streaming using spectral domain phase microscopy, *J. Biomed. Opt.* **11**(2), 024014 (2006).
- [6] A. K. Ellerbee, T. L. Creazzo, and J. A. Izatt, Investigating nanoscale cellular dynamics with cross-sectional spectral domain phase microscopy, *Opt. Express* **15**(13), 8115–8124 (2007).
- [7] <http://en.wikipedia.org/wiki/Physarum>
- [8] K. E. Wohlfarth-Bottermann, Plasmalemma invaginations as characteristic constituents of plasmodia of *Physarum polycephalum*, *J. Cell Sci.* **16**, 23–37 (1974).
- [9] Yu. M. Romanovskii and V. A. Teplov, The physical bases of cell movement. The mechanisms of self-organisation of amoeboid motility, *Phys. Usp.* **38**, 521–542 (1995).
- [10] A. V. Priezzhev, M. V. Evdokimov, and Yu. M. Romanovskii, Rayleigh spectroscopy of biological objects, *Sov. J. Quantum Electron.* **8**(12), 2600–2608 (1981).
- [11] S. Takagi and T. Ueda, Emergence and transitions of dynamic patterns of thickness oscillation of the plasmodium of the true slime mold *Physarum polycephalum*, *Physica D* **237**, 420–427 (2008).
- [12] R. Kobayashi, A. Tero, and T. Nakagaki, Mathematical model for rhythmic protoplasmic movement in the true slime mold, *J. Math. Biol.* **53**, 273–286 (2006).
- [13] J. Lauri, M. Wang, M. Kinnunen, and R. Myllylä, Measurement of microfluidic flow velocity profile with two Doppler optical coherence tomography systems, *Proc. SPIE* **6863**, 68630F (2008).
- [14] E. S. Castle, The refractive indices of whole cells, *J. Gen. Physiol.* **17**(1), 41–47 (1933).
- [15] W. G. Camp, A method of cultivating myxomycete plasmodium, *Bull. Torrey Bot. Club* **36**, 205 (1936).
- [16] P. E. Andersen, L. Thrane, H. T. Yura, A. Tycho, and T. M. Jorgensen, Optical coherence tomography: advanced modeling, in: *Handbook of Coherent Domain Optical Methods*, ed. by V. V. Tuchin, Vol. 2 (Kluwer Academic, Boston, 2004), pp. 61–118.
- [17] D. Levitz, L. Thrane, M. H. Frosz, P. E. Andersen, C. B. Andersen, J. Valanciunaite, J. Swartling, S. Andersson-Engels, and P. R. Hansen, Determination of optical scattering properties of highly-scattering media in optical coherence tomography images, *Opt. Express* **12**(2) 249–259 (2004).
- [18] I. V. Turchin, E. A. Sergeeva, L. S. Dolin, and V. A. Kamensky, Estimation of biotissue scattering properties from OCT images using a small-angle approximation of transport theory, *Laser Phys.* **13**(12), 1524–1529 (2003).
- [19] D. P. Popescu and M. G. Sowa, In vitro assessment of optical properties of blood by applying the extended Huygens–Fresnel principle to time-domain optical coherence tomography signal at 1300 nm, *Int. J. Biomed. Imaging* **2008**, 1–6 (2008).
- [20] K. V. Larin, M. Motamedi, T. V. Ashitkov, and R. O. Esenaliev, Specificity of noninvasive blood glucose sensing using optical coherence tomography technique: a pilot study, *Phys. Med. Biol.* **48**, 1371–1390 (2003).
- [21] R. V. Kuranov, V. V. Sapozhnikova, D. S. Prough, I. Ciceaite, and R. O. Esenaliev, *In vivo* study of glucose-induced changes in skin properties assessed with optical coherence tomography, *Phys. Med. Biol.* **51**, 3885–3900 (2006).
- [22] S. T. Flock, S. L. Jacques, B. C. Wilson, W. M. Star, and M. J. C. van Gemert, Optical properties of Intralipid: a phantom medium for light propagation studies, *Lasers Surg. Med.* **12**, 510–519 (1992).
- [23] H. J. van Staveren, C. J. M. Moes, J. van Marie, S. A. Prahl, and M. J. C. van Gemert, Light scattering in Intralipid-10% in the wavelength range of 400–1100 nm, *Appl. Opt.* **30**(31), 4507–4514 (1991).